Low-Energy Impact Dynamics in the Earth – Moon System ⋆

Elisa Maria Alessi * **Gerard Gómez** ** **Josep J. Masdemont** ***

* *IEEC & Dpt. Matemàtica Aplicada i Anàlisi, Universitat de Barcelona, Gran Via 585, 08007 Barcelona, Spain. (e-mail: elim@maia.ub.es).*
** *IEEC & Dpt. Matemàtica Aplicada i Anàlisi, Universitat de Barcelona, Gran Via 585, 08007 Barcelona, Spain. (e-mail: gerard@maia.ub.es)*
*** *IEEC & Dpt. Matemàtica Aplicada I, Universitat Politècnica de Catalunya, Diagonal 647, 08028 Barcelona, Spain. (e-mail: josep@barquins.upc.edu)*

Abstract: Most of the craters on the surface of the Moon were created by the collision of minor bodies of the Solar System, in particular asteroids coming from the Main Belt as a consequence of different types of resonance. Our aim is to investigate the dynamics of such asteroids, paying special attention on the hyperbolic invariant manifolds associated with the equilibrium point L_2 of the Earth – Moon system within the framework of the Circular Restricted Three – Body Problem. We analyze how different distributions of initial conditions for transit trajectories and the value considered for the relative Earth – Moon distance can vary the probability of a lunar impact. Then, we add the gravitational effect of the Sun by means of the Bicircular Restricted Four – Body Problem, showing that the initial phase associated with the Sun and the ratio between the Earth – Moon – Sun distance and the Earth – Moon one can affect the collision pattern in terms of lunar longitude and latitude.

Keywords: CR3BP, Invariant Manifolds, Lunar Craters.

1. INTRODUCTION

In this work we will cope with the collision of asteroids onto the Moon. Such phenomenon takes place continuously on all the rocky planets and satellites populating the Solar System, as it can be inferred from the craters that mould their surface.

There exists a huge literature (see, for instance, Melosh (1999); Neukum et al. (2001); Morota, Furumoto (2003); Le Feuvre (2008); Marchi et al. (2009)) devoted to the cratering process, because it provides information on the chronology of the target body, on the impacting asteroids and thus on the Solar System evolution, not only in dynamical terms but also in astronomical and geological ones. Our aim is far from deriving a complete comprehension of this kind of events, but we are interested in supplying a different methodology that can aid in this way.

We will address the problem of the role played by low-energy trajectories in the creation of lunar impact craters, asking whether they produce a specific distribution of collisions, for instance on the farside of the Moon, when considering a particular range of energies.

Within the approximation of the Circular Restricted Three – Body Problem, we will simulate the behavior of transit trajectories lying inside the stable invariant manifold associated with the central invariant manifold of the collinear equilibrium point L_2. Since the most intense bombardment on the Moon happened between 4 and 3.8 Gy ago, we will analyze several values for the Earth – Moon distance. Also, we will see if the choice of the dissemination of initial conditions can affect the final outcome.

Then, we will exploit the Bicircular Restricted Four – Body Problem in order to understand how the influence of the Sun can affect trajectories derived in the above way.

2. THE CIRCULAR RESTRICTED THREE – BODY PROBLEM

The Circular Restricted Three – Body Problem (CR3BP) (Szebehely, 1967) studies the behavior of a particle P with infinitesimal mass m_3 moving under the gravitational attraction of two primaries P_1 and P_2, of masses m_1 and m_2, revolving around their center of mass on circular orbits.

To remove time from the equations of motion, it is convenient to introduce a synodic reference system $\{O, x, y, z\}$, which rotates around the $z-$axis with constant angular velocity ω equal to the mean motion n of the primaries. The origin of the reference frame is set at the barycenter of the system and the $x-$axis on the line which joins the primaries, oriented in the direction of the largest primary.

⋆ This work has been supported by the Spanish grants MTM2006–05849 (E.M.A., G.G.), MTM2009–06973 and 2009SGR859 (J.J.M.) and by the Astronet Marie Curie fellowship (E.M.A.).

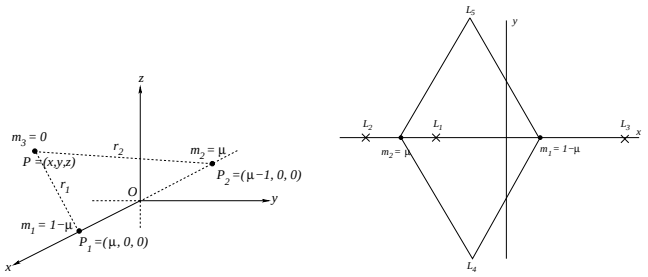

Fig. 1. Left: the Circular Restricted Three-Body Problem in the synodical reference system with adimensional units. Right: The five equilibrium points associated with the problem.

In this way we work with m_1 and m_2 fixed on the $x-$axis, as shown in Fig. 1.

The units are chosen to set the gravitational constant, the sum of the masses of the primaries, the distance between them and the modulus of the angular velocity of the rotating frame to be unitary. For the Earth – Moon system, the unit of distance equals 384400 km, the unit of velocity equals 1.02316 km/s and the dimensionless mass of the Moon is $\mu = \frac{m_2}{m_1+m_2} = 0.012150582$. With these reference system and units, the equations of motion can be written as

$$\begin{aligned} \ddot{x} - 2\dot{y} = \frac{\partial \Omega}{\partial x} &= x - \frac{(1-\mu)}{r_1^3}(x-\mu) - \frac{\mu}{r_2^3}(x+1-\mu), \\ \ddot{y} + 2\dot{x} = \frac{\partial \Omega}{\partial y} &= y - \frac{(1-\mu)}{r_1^3}y - \frac{\mu}{r_2^3}y, \\ \ddot{z} = \frac{\partial \Omega}{\partial z} &= -\frac{(1-\mu)}{r_1^3}z - \frac{\mu}{r_2^3}z, \end{aligned} \tag{1}$$

where

$$\Omega(x,y,z) = \frac{1}{2}(x^2+y^2) + \frac{1-\mu}{r_1} + \frac{\mu}{r_2} + \frac{1}{2}(1-\mu)\mu,$$

and $r_1 = [(x-\mu)^2+y^2+z^2]^{\frac{1}{2}}$ and $r_2 = [(x+1-\mu)^2+y^2+z^2]^{\frac{1}{2}}$ are the distances from P to P_1 and P_2, respectively.

System (1) has a first integral, the *Jacobi integral*, which is given by

$$2\Omega(x,y,z) - \left(\dot{x}^2+\dot{y}^2+\dot{z}^2\right) = C, \tag{2}$$

where C is the so called Jacobi constant.

In the synodic reference system, there exist five equilibrium (or libration) points. Three of them, the *collinear* ones, are in the line joining the primaries and are usually denoted by L_1, L_2 and L_3. The other two equilibrium points, L_4 and L_5, the *triangular* ones, are in the plane of motion of the primaries and form an equilateral triangle with them. See Fig. 1.

If C_i $(i = 1, \ldots, 5)$ denotes the value of the Jacobi constant at the L_i equilibrium point, it holds that

$$C_1 > C_2 > C_3 > C_4 = C_5 = 3.$$

Depending on the value of the Jacobi constant, it is possible to know where the particle can move in the configuration space. According to (2), the regions where the motion is forbidden are the *zero-velocity surfaces*. For a given value of the mass parameter, there exist five different geometric configurations, four of them displayed in 2.

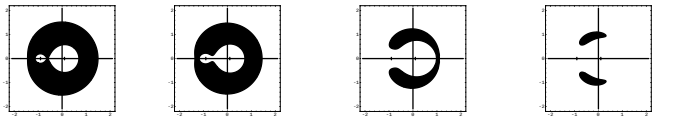

$C > C_1$ $\quad C_2 < C < C_1$ $\quad C_3 < C < C_2$ $\quad C_4 < C < C_3$

Fig. 2. Intersection of the zero-velocity surfaces with the $\{z = 0\}$ plane for $\mu > 0$. The motion is forbidden in the filled areas. The case $C < C_4 = C_5$ is not displayed since the motion is allowed everywhere.

2.1 Central and Hyperbolic Invariant Manifolds

The collinear libration points behave, linearly, as the product of two centers by a saddle. This means that around a collinear point we deal with bounded orbits, which are due to the central part and also with escape trajectories, which depart exponentially from the neighborhood of the collinear point for $t \to \pm\infty$ and are due to the saddle component. The former kind of motion belongs to the *central invariant manifold* $\mathcal{W}^c(L_i)$, the latter to the *hyperbolic invariant manifolds* associated with the central invariant one. The hyperbolic manifolds consist, in particular, in one stable and one unstable, $\mathcal{W}^s(L_i)$ and $\mathcal{W}^u(L_i)$ respectively.

Eeach type of central orbit around a collinear point has a stable and an unstable invariant manifold. Each manifold has two branches, a positive and a negative one. They look like tubes (empty or solid) of asymptotic trajectories tending to, or departing from, the corresponding orbit. These tubes have a key role in the study of the natural dynamics of the libration regions. When going forwards in time, the trajectories on the stable manifold approach exponentially the periodic/quasi-periodic orbit, while those on the unstable manifold depart exponentially. As a matter of fact (Conley, 1968; Llibre et al., 1985; Gómez et al., 2004), these orbits separate two types of motion. The *transit* solutions are those orbits belonging to the interior of the manifold and passing from one region to another. The *non-transit* ones are those staying outside the tube and bouncing back to their departure region.

We refer to the stable(/unstable) invariant manifold associated with the central invariant manifold of a given equilibrium point $\mathcal{W}^{s/u}(\mathcal{W}^c_{L_i})$ $(i = 1, 2, 3)$ as the union of the stable(/unstable) manifolds associated with each type of periodic and quasi-periodic orbits.

Transit Orbits Computation. In principle, one can compute transit trajectories starting from a given kind of periodic or quasi-periodic orbit. However, for a given level of energy we determine $\mathcal{W}^{s/u}(\mathcal{W}^c_{L_i})$ $(i = 1, 2, 3)$ using only the hyperbolic invariant manifolds corresponding to the planar and vertical periodic orbits, $\mathcal{W}^{s/u}(PL_{L_i})$ and $\mathcal{W}^{s/u}(VL_{L_i})$ $(i = 1, 2, 3)$ respectively, which exist for the well-defined value of C. Indeed, planar and vertical Lyapunov orbits act as energy boundaries for transit orbits lying inside $\mathcal{W}^{s/u}(\mathcal{W}^c_{L_i})$, namely,

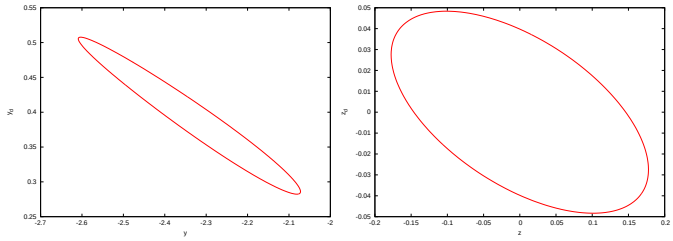

Fig. 3. $(y, \dot{y})$ and $(z, \dot{z})$ curves where we pick up initial conditions for transit orbits of $\mathcal{W}^s(\mathcal{W}^c_{L_2})$.

$$\mathcal{W}^{s/u}(\mathcal{W}^c_{L_i}) \subset \mathcal{W}^{s/u}(PL_{L_i}) \times \mathcal{W}^{s/u}(VL_{L_i}) \quad (i = 1, 2, 3). \tag{3}$$

2.2 $\mathcal{W}^s(\mathcal{W}^c_{L_2})$ as Impact Gate

To study the role that low-energy orbits might have in the formation of lunar impact craters, we assume as main channel to get to the Moon the stable invariant manifold associated with the central invariant manifold around the L_2 point. This hypothesis is based on the fact that we admit as energy levels only those belonging to the third regime depicted in Fig. 2.

More precisely, we focus on the behaviour of transit trajectories belonging to $\mathcal{W}^s(\mathcal{W}^c_{L_2})$ for $C_3 < C < C_2$, that is, $C \in (3.024150, 3.184163)$. We want to figure out if there exists a specific distribution of impact brought by this kind of dynamics, without forgetting that the relative distance between Earth and Moon, say d_{EM}, could affect the total outcome, as well as the distribution of initial conditions.

First, we have to consider that the more intense lunar bombardment took place some billions years ago and that the Moon is receding from the Earth. As the rate of recession has not been constant in the past and it did not behave linearly either, we take 4 values for d_{EM}: 232400, 270400, 308400, 384400 km, respectively. According to Le Feuvre (2008), they correspond approximately to 4., 3.4, 2.5 and 0 Gy ago.

With respect to the initial conditions, in a given level of energy the dynamics corresponding to $\mathcal{W}^s(\mathcal{W}^c_{L_2})$ is determined starting from the invariant stable manifolds of the planar and vertical Lyapunov periodic orbits existing around L_2. In particular, we propagate these manifolds backwards in time until they cross a given section for the first time. We consider the branch which moves away from the Moon and the plane of intersection is chosen in such a way that we can assume the asteroids to have already left the Main Asteroid Belt and to move in the Earth – Moon neighborhood.

The transit trajectories are generated by taking initial positions and velocities inside the two closed curves we obtain in this way. If the chosen section is, for example, $\{x = 0\}$, then we deal with a closed curve in the $(y, \dot{y})$ plane and one in the $(z, \dot{z})$ plane (see Fig. 3). The x component is determined by the fixed section, the $\dot{x}$ one by C.

In what follows, we describe how the points at $t = 0$ are taken using 4 different strategies and the corresponding results. All the random variables needed are derived by

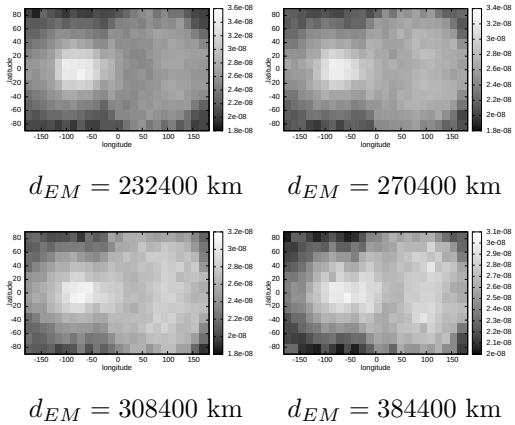

$d_{EM} = 232400$ km $\quad$ $d_{EM} = 270400$ km

$d_{EM} = 308400$ km $\quad$ $d_{EM} = 384400$ km

Fig. 4. Density of impact (number of impacts per unit of area normalized with respect to the total number of impacts obtained) computed by exploiting the CR3BP equations of motion and initial conditions uniformly distributed inside $\mathcal{W}^s(\mathcal{W}^c_{L_2})$. The color bar indicates that the lighter the shade of gray the greater the impact density.

means of a Knuth shuffle algorithm (Knuth, 1997). We consider 20 equally spaced energy levels C in the range $C_3 < C < C_2$. We notice that the smaller the value of C, the larger the two curves.

The methodology adopted consists in integrating numerically the equations of motion of the CR3BP forwards in time starting from such initial states. The maximum allowed time for impacting onto the surface of the Moon is 60 years, provided the assumption of a no longer life in the region under consideration. If a trajectory collides with the Moon we calculate the longitude and latitude corresponding to the site of impact, together with the velocity and the angle of arrival. The distributions of impact on the Moon is represented by discretizing the lunar spherical surface in squares of $15° \times 15°$ in terms of longitude and latitude. According to the number of collisions per unit of area, normalized with respect to the total number of impacts obtained, each square can assume a different shade of gray: in the figures we will show the lighter it is the greater the density of impact.

Generally speaking, the minor bodies can behave in one of the following ways:

- they collide with the Moon without overcoming the L_1 border;
- they collide with the Moon after overcoming the L_1 border and thus performing several loops around the Earth;
- they keep wandering around the Earth inside the area delimited by the zero-velocity surface;
- they escape from the Earth – Moon neighborhood just after jumping on the L_2 gate;
- they exit from the Earth – Moon neighborhood after wandering for a certain interval of time around the Earth.

Note that just the first two cases cause the formation of craters of impact on the surface of the Moon.

In general, we notice that to assume 60 years as maximum allowed time to impact is not a restrictive condition. In the

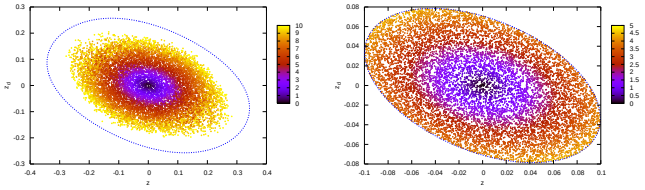

Fig. 5. The two plots show the $(z, \dot{z})$ curve at the intersection for $C = 3.043549$ (left) and $C = 3.171551$ (right). The points inside are initial conditions corresponding to $i \in [0°, 10°]$, as indicated by the color bar.

time interval considered the most of the asteroids escapes from the region we are interested in and it looks like just few of them are able to go back to the Earth – Moon neighborhood later. It is reasonable to think that they remain in the Inner Solar System and occasionally are pushed towards the Earth again.

Concerning the velocity of arrival, it almost coincides with the velocity of escape of the Moon. The angle of impact can assume all the values between 0° and 90°.

To Be Uniform in $\mathcal{W}^s(\mathcal{W}^c_{L_2}$.) The first selection of initial states inside the Poincaré section we study is an uniform distribution inside each curve produced by $\mathcal{W}^s(PL_{L_2})$ and $\mathcal{W}^s(VL_{L_2})$. This means that we want any transit trajectory inside the tube to be as probable as any other. For each energy level we analyze the behaviour of 10^6 initial conditions.

We can point out the following outcomes:

- the percentage of impacting orbits over all the initial conditions launched goes from 13% for $d_{EM} = 384400$ km up to 18% for $d_{EM} = 232400$ km;
- the amount of particles that still wander around the Earth inside the zone bounded by the zero-velocity surface after 60 years is 0.1%;
- most of the impacts take place within 20 years, though in the first 10 years we observe the greatest number;
- the heaviest probability of impact takes place at the apex of the lunar surface $(90°W, 0°)$.

In Fig. 4, we show the density of impact found for the 4 values of d_{EM} introduced previously.

To Belong to the Ecliptic. To each initial condition we consider in a given section we can associate an orbital inclination, say i, with respect to the Earth, provided the fact to be not too close to the Moon. First, we have to move to an inertial system of coordinates whose reference plane is the Earth – Moon orbital one and whose origin is set at the Earth and then perform a classical transformation to orbital elements (see, for instance, Bate et al. (1971)).

We implement this procedure in order to understand how orbits coming from the ecliptic can affect the distributions of impacts on the Moon. Therefore, the second set of initial conditions we consider to propagate is selected according to i. In particular, we accept those associated with a value of $i < 10°$. We recall that the ecliptic lies at about $5°14'$ with respect to the Moon's orbit.

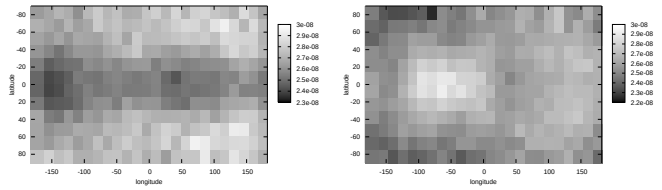

$i \in [3°, 7°]$ $\qquad$ $i \in [0°, 10°]$

Fig. 6. Density of impact produced by initial conditions selected according to the inclination i of the associated osculating ellipse. $d_{EM} = 384400$ km. The color bar indicates that the lighter the shade of gray the greater the impact density.

Also in this exploration, for each energy level we analyze the behaviour of 10^6 initial conditions.

First of all, we notice that as long as C decreases, that is, the particle becomes more and more energetic, the range of possible i increases. In the $(z, \dot{z})$ curve, the closer the point to the center the lower the inclination (see Fig. 5). In turn, the choice of i results essentially in the area covered by the initial conditions inside the $(z, \dot{z})$ projection: to skip high values of i means to neglect the neighborhood of the $(z, \dot{z})$ boundary, to avoid values of i close to 0° signifies to not sweep the center of the $(z, \dot{z})$ curve's interior.

As a consequence, the range of admitted i affects the distribution of lunar impacts. In Fig. 6, we show the density of impact obtained setting $i \in [3°, 7°]$ and $i \in [0°, 10°]$. We can notice that we obtain a lower density around 0° latitudes in the first case than in the other. Indeed, almost planar transit orbits yield to impacts focused on the lunar equator. Moreover, the more comprehensive set of i maintains the apex concentration previously observed.

To Be in Resonance with the Moon. Another possibility we want to explore is the effect of a hypothetical resonance between the Moon and the asteroid. It is known that if two bodies experience close approaches repeatedly in time, the consequent gravitational perturbations accumulate, bringing the orbits to change drastically. On the contrary, if the resonance and the initial configuration are such that the two bodies will never encounter, then the system is somehow protected.

We say that an asteroid is in resonance with respect to the Moon at $t = 0$ if

$$n_a T_a = n_M T_M, \tag{4}$$

where $n_a, n_M \in \mathbb{N}_+$ and T_a and T_M are the orbital periods of the asteroid and the Moon with respect to the Earth. As $T_a = \sqrt{a^3 4\pi^2 \mu_2}$, where a is the semi-major axis and $\mu_2 = 1 - \mu$, we propagate forwards in time only the initial conditions which satisfy

$$a = (\mu_2)^{1/3} \left(\frac{n_M}{n_a} \right)^{2/3}. \tag{5}$$

We notice that we always have $n_a > n_M$, as the asteroids are assumed to move outside the orbit of the Moon.

For this simulation, we take 10^6 initial conditions for each energy value.

The outcome reveals a distribution of impacts very similar to the ones found above. This means that a relative Moon – asteroid configuration which repeats in time does not influence the possibility of collision when the stable component of the central invariant manifold of a given equilibrium point controls the dynamics. We note that we take into account a quite diverse series of initial resonances and that in most of the cases they break up quite soon and transform into different ones such that $n_a < n_M$.

To Be Uniform in C. To the fourth distribution of initial conditions we ask to be uniform in a given level of energy. Due to the existence of the Jacobi integral of motion, there exists a 5−dimensional surface, say $\mathcal{M}$, embedded in the 6−dimensional Euclidean space we deal with.

For any well-defined C the embedding of $\mathcal{M}$ is given by the map $J : \mathbb{R}^5 \to \mathbb{R}^6$ defined as

$$\begin{aligned}
J_1(x,y,z,\dot{y},\dot{z}) &= x,\\
J_2(x,y,z,\dot{y},\dot{z}) &= y,\\
J_3(x,y,z,\dot{y},\dot{z}) &= z,\\
J_4(x,y,z,\dot{y},\dot{z}) &= x^2+y^2+2\frac{1-\mu}{r_1}+2\frac{\mu}{r_2}+\mu(1-\mu)\\
&\quad -\dot{y}^2-\dot{z}^2-C,\\
J_5(x,y,z,\dot{y},\dot{z}) &= \dot{y},\\
J_6(x,y,z,\dot{y},\dot{z}) &= \dot{z}.
\end{aligned} \tag{6}$$

Our purpose is to set the same density of initial conditions per unit of element of volume on $\mathcal{M}$. This is,

$$\frac{\#\quad points}{element\quad of\quad volume} = constant. \tag{7}$$

The constant above, say χ, is fixed and the element of volume is computed by means of the basis of vectors which generates the tangent space of $\mathcal{M}$, say $\mathcal{T}_{\mathcal{C}}\mathcal{M}$.

Actually we have to calculate a 4−dimensional element of volume, because of the choice of the Poincaré section, which determines the value of x. Let $u \equiv (x,y,z,\dot{y},\dot{z})$, then the basis of $\mathcal{T}_{\mathcal{C}}\mathcal{M}$ is given by $(\frac{\partial J_k}{\partial u_i})$, where $k = 1,\ldots,6$ and $i = 2,\ldots,5$. For a given u^*, the element of volume is the determinant of the matrix $V = [g_{ij}]$, where

$$g_{ij} = \sum_{k=1}^{6} \frac{\partial J_k}{\partial u_i}\frac{\partial J_k}{\partial u_j}(u^*), \qquad i,j = 2,\ldots,5. \tag{8}$$

For further details, see Do Carmo (1992).

The last type of initial conditions reserves a sort of surprise, as they do not provide the same density of impact encountered with all the previous explorations. The percentage of impact oscillates between 4% and 7% and it seems that the apex focusing is now shifted westward around $(130°W, 0°)$ and that many collisions on the lunar east side are lost.

3. THE BICIRCULAR RESTRICTED FOUR – BODY PROBLEM

As we are aware that the influence of the Sun plays a significant role on the dynamics which takes place in the Earth – Moon framework, we review the outcome obtained with the CR3BP model by assuming the Bicircular Restricted Four – Body Problem (BR4BP) (Cronin et al., 1964). The main difference between the two models is that in the latter neither equilibrium points nor first integrals exist. Actually, it does not represent a realistic model of forces, in the sense that Earth, Moon and Sun do not follow the Newtonian law. Though it is a mathematical construction, the BR4BP is helpful to get an insight of the consequences that the presence of the Sun can take.

The BR4BP considers the infinitesimal mass P to be affected by the gravitational attractions of three primaries. Earth and Moon revolve in circular orbits around their common center of mass and, at the same time, this barycenter and the Sun move on circular orbits around the center of mass of the Earth – Moon – Sun system.

The usual framework to deal with is the synodical reference system with origin at the Earth – Moon barycenter: in this way Earth and Moon are fixed on the x−axis as before and the Sun is supposed turning clockwise around the origin.

Let us take adimensional units as in the CR3BP and let $m_S = 328900.5614$ be the mass of the Sun in such units, a_S be the distance between the Earth – Moon barycenter and the Sun, ω be the mean angular velocity of the Sun in synodical coordinates and θ_0 be the value associated with the rotation of the Sun with respect to the Earth – Moon barycenter at $t = 0$.

If $\theta = \omega t$, then the position of the Sun is described by

$$\begin{aligned}
x_S &= a_S\cos(\theta-\theta_0),\\
y_S &= -a_S\sin(\theta-\theta_0),
\end{aligned} \tag{9}$$

and the equations of motion for the particle P can be written as

$$\begin{aligned}
\ddot{x}-2\dot{y} =&\ x-\frac{(1-\mu)}{r_1^3}(x-\mu)-\frac{\mu}{r_2^3}(x+1-\mu)\\
&-(x-x_S)\frac{m_S}{r_S^3}-\cos(\theta-\theta_0)\frac{m_S}{a_S^2},\\
\ddot{y}+2\dot{x} =&\ y-\frac{(1-\mu)}{r_1^3}y-\frac{\mu}{r_2^3}y-(y-y_S)\frac{m_S}{r_S^3}\\
&-\sin(\theta-\theta_0)\frac{m_S}{a_S^2},\\
\ddot{z} =&\ -\frac{(1-\mu)}{r_1^3}z-\frac{\mu}{r_2^3}z-z\frac{m_S}{r_S^3},
\end{aligned} \tag{10}$$

where μ has the same meaning and value as before and $r_1 = [(x-\mu)^2+y^2+z^2]^{\frac{1}{2}}$, $r_2 = [(x+1-\mu)^2+y^2+z^2]^{\frac{1}{2}}$, $r_S = [(x-x_S)^2+(y-y_S)^2+z^2]^{\frac{1}{2}}$ are the distances from P to Earth, Moon and Sun, respectively.

3.1 Numerical Results

We focus on the most relevant concentration of impact on the leading side of the Moon obtained with uniformly distributed transit orbits and we apply the BR4BP equations of motion to the same initial conditions considered within the CR3BP framework.

Also in this case, we are able to attribute to d_{EM} some specific values, which account for the rate of recession

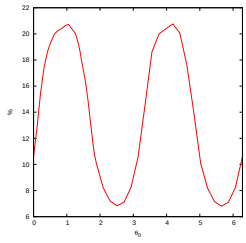

Fig. 7. Percentage of impact as a function of θ_0, for $d_{EM} = 270400$ km.

of the Moon with respect to the Earth. We notice that a_S and ω change accordingly to d_{EM}, as we assume the adimensional set of units.

The simulation is carried on as in Section 2.2, apart from the fact that now we have to explore the behaviour corresponding to different θ_0 and that we have to take care of impacts on the surface of the Earth. Finally, the maximum time span we allow to give birth to a lunar collision is 5 years. This choice is essentially due to the increasing computational effort.

The results obtained can be summarized as follows:

- some trajectories collide with the Earth;
- the percentage of impact on the Moon depends on d_{EM} and on the initial phase of the Sun, θ_0. In particular, according to θ_0 the percentage of impact follows a periodic pattern (see Fig. 7);
- it looks like the Sun, depending on θ_0, is able to prevent the particle from entering into the region that was delimitated by the zero-velocity surface in the CR3BP case;
- the relative Earth – Moon and Earth – Moon – Sun distances, as well as the adimensional diameter of the Moon, play a significant role in what concerns with the region of heaviest lunar impact. In particular, the leading side collision concentration becomes more and more evident as d_{EM} decreases, while the highest density of impact oscillates in longitude in the range $[50°W, 100°W]$ depending on θ_0.
- The effect of the Sun reduces the number of impacts on the trailing side of the Moon, which is quite high when only Earth and Moon are considered.

4. CONCLUSIONS

From the exploitation of the CR3BP approximation, it turns out that transit orbits which are uniformly distributed inside $\mathcal{W}^s(\mathcal{W}^c_{L_2})$ gives rise to more intense collisions in the neighborhood of the apex of the surface of the Moon. If we modify the initial inclination with respect to the Earth – Moon orbital plane of the orbits propagated this phenomenon can change.

On the other hand, if the impactors were uniformly distributed inside a specific range of energy, then a very low percentage of crashes would happen on the lunar east side and the major focusing would take place at a different longitude than before.

The gravitational force exerted by the Sun seems to blur the leading side concentration experienced under the CR3BP. Changing the ratio between the Earth – Moon – Sun distance and the Earth – Moon one, we notice different patterns. Moreover, we get evidence that the position of the Sun at the initial epoch with respect to the Earth – Moon barycenter affects the distribution of impact. Indeed, we notice that, according to θ_0, the percentage of impact changes in a periodic way and also the region of largest density swings in longitude.

ACKNOWLEDGEMENTS

We acknowledge the use of the UPC Applied Math cluster system for research computing.
See http://www.ma1.upc.edu/eixam/index.html

REFERENCES

R.R. Bate, D.D. Mueller, J.E. White. *Fundamental of Astrodynamics*. Dover Publications, Inc., New York, 1971.

C. Conley. Low energy transit orbits in the restricted three-body problem. *SIAM Journal on Applied Mathematics*, 16, 732–746, 1968.

J. Cronin, P.B. Richards, L.H. Russell. Some periodic solutions of a four-body problem. *Icarus*, 3 423–428, 1964.

M.P. Do Carmo. *Riemannian Geometry*. Birkhäuser, Boston, 1992.

G. Gómez, W.S. Koon, M.W. Lo, J.E. Marsden, J. Masdemont, S. Ross. Connecting Orbits and Invariant Manifolds in the Spatial Restricted Three–Body Problem. *Nonlinearity*, 17 1571–1606, 2004.

D.E. Knuth. *The Art of Computer Programming – Volume* 1. Addison – Wesley, Reading, Massachusetts, 1997.

M. Le Feuvre. Modéliser le bombardement des planètes et des lunes. Application à la datation par comptage des cratères. *Ph.D Thesis*, Institut de Physique du Globe de Paris, 2008.

J. Llibre, R. Martínez, C. Simó. Transversality of the Invariant Manifolds associated to the Lyapunov Family of Periodic Orbits near L_2 in the Restricted Three Body – Problem. *Journal of Differential Equations*, 58 104–156, 1985.

S. Marchi, S. Mottola, G. Cremonese, M. Massironi, E. Martellato. A new chronology for the Moon and Mercury. *The Astronomical Journal*, 137, 4936–4948, 2009.

H.J. Melosh. *Impact Cratering*. Oxford University Press, New York, 1999.

T. Morota, M. Furumoto. Asymmetrical Distribution of Rayed Craters on the Moon. *Earth and Planetary Science Letters* 206, 315–323, 2003.

H. Neukum, B.A. Ivanov, W.K. Hartmann. Cratering Records in the Inner Solar System in relation to the Lunar Reference System. *Chronology and Evolution of Mars*, 96, 55–86, 2001.

V. Szebehely. *Theory of orbits*. Academic Press, New York, 1967.